Hydrogen Stark Broadening by Different Kinds of Model Microfields

Joachim Seidel
Institut für Theoretische Physik der Universität Düsseldorf

Z. Naturforsch. **35a**, 679–689 (1980); received April 3, 1980

The "method of model microfields (MMM)", which has been employed successfully especially for the calculation of hydrogen Stark profiles, is based on the assumption that reliable line shapes may be obtained from just the probability density of the plasma microfield and its autocorrelation function. To test the influence of higher order statistical features two different model microfields have been used to investigate Stark broadening of hydrogen Lyman lines by either electrons or ions. Corresponding profiles computed in this way lie close together over the full intensity range, but systematic relative deviations of about 20% show up at frequency separations from the unperturbed line of approximately three times the plasma frequency (for electrons or ions, respectively), i.e., in the "transition region" where neither the impact nor the static approximation holds. Though the joint action of electrons and ions as well as Doppler broadening will tend to diminish these deviations, the present form of the MMM cannot be expected to yield an accuracy better than some 10% throughout the line profile.

1. Introduction

Until recently, hydrogen Stark profiles have always been calculated with the aid of the "(quasi-) static approximation" for the perturbing plasma ions which has been used by Holtsmark [1] in 1919 for the first time. Theoretical estimates seemed to prove that this approximation is fully appropriate to describe the effects of the low frequency ionic part of the plasma microfield, and only small errors were expected to result from it for laboratory plasmas [2]. During the last years, however, convincing experimental evidence has been found for distinct "ion dynamical effects" in the cores of hydrogen lines. Kelleher and Wiese [3] and Wiese et al. [4] demonstrated a marked dependence of the central structure of Balmer lines on the reduced mass of the radiating atom — perturbing ion pair, and other experiments have confirmed their findings for different plasma conditions [5–9]. In addition, Grützmacher and Wende [10] succeeded for the first time in measuring the central part of L_α from an optically thin plasma; they found a line width greatly exceeding the theoretical value calculated with static ions [2, 11]. Another experiment [12] on L_β revealed less structure in the line centre than theoretically predicted, too, and a recent numerical simulation [13] corroborates the conjecture that the neglect of ion dynamics in the usual theoretical treatment is responsible for at least the main part of the discrepancies.

To explain these experimental results, various theoretical approaches [14–22] have been elaborated since which try to account approximately for the effects of relative emitter-ion motion on hydrogen Stark broadening. Most of these calculations yield profiles which coincide quite closely or even perfectly with the L_α profiles recorded by Grützmacher and Wende. However, satisfactory agreement with all experimental data which are available by now has been achieved solely by "model microfield calculations" [17]. The "model microfield method (MMM)" — introduced by Brissaud and Frisch [23, 24] — has been applied successfully to nonhydrogenic lines as well [25, 26]; it has the distinction of providing a nonperturbative many-body (microfield) treatment of Stark broadening which seems to be well suited for the broadening of hydrogen lines by plasma ions [27].

Despite of its considerable success, there is a shortcoming of the MMM impeding its more widespread acceptance as a powerful tool in line broadening calculations: In general, no error estimate is known for the method, and it is hard to see how it should be improved to get still closer to the exact solution. With regard to electron broadening of hydrogen lines, the validity of the MMM has been demonstrated by comparison [28] with the results of the "unified theory" [11], and there are other

Reprint requests to the author's new address: Dr. J. Seidel, Physikalisch-Technische Bundesanstalt, Institut Berlin, Abbestr. 2–12, D-1000 Berlin 10.

0340-4811 / 80 / 0700-0679 $ 01.00/0. — Please order a reprint rather than making your own copy.

examples of stochastic differential equations where the MMM approximation works excellently [24]. In the case of ion dynamical effects, however, the main justification of the method is the good overall agreement with the experimental data. For that reason, it would be highly desirable to have some means to value the reliability of the MMM without taking recourse to results from outside, experimental or theoretical.

In this paper, I try to give an estimate of the uncertainties adhering to the MMM by computing line profiles with different model microfields. These models coincide with one another (and with the true plasma microfield) as far as the instantaneous probability distribution $P(\boldsymbol{E})$ and the autocorrelation function $\Gamma(t)$ of the microfield are concerned, but they differ in more complicated statistical features to allow for an appraisal of the influence which the latter have on the line profile. (The MMM is based on the assumption that reliable line profiles may be calculated from P and Γ alone, while higher order statistical features of the microfield are less important in this context.) Indeed, it is possible to do this in the frame of the MMM: Though all previous calculations have used the so-called "kangaroo process (KP)" [23] as model microfield, a more general version of the MMM is available [24, 28, 29] which utilizes a "renewal process (RP)" instead. (The KP is just the special Markovian case of the RP.) Accordingly, there are even infinitely many model microfields beside the KP for which exact line profiles are known in principle.

In Sect. 2, I shall recapitulate the essential features of the general form of the MMM. Then, a novel model microfield is defined, the "theta process (TP)", which is the "most non-Markovian" RP and hence constitutes the opposite of the KP in this respect. TP and KP will be used to demonstrate the effects of different model microfields on hydrogen line profiles. The calculations are most easily done for the Lyman lines, and for the present purpose it will be sufficient to study just these. Moreover, electron broadening will certainly hide small differences in ion broadening and vice versa, so it is appropriate to investigate the two kinds of Stark broadening separately. The Lyman line profiles take on comparatively simple forms then, as will be shown in Section 3. Numerical results are presented in Sect. 4, and Sect. 5 at last contains a summary and the conclusions.

2. The Method of Model Microfields

2.1. Point of departure

Under suitable approximations [2], the Stark profile of a hydrogen resonance line is

$$I(\Delta\omega) \propto \mathrm{Re} \int_0^\infty \mathrm{d}t\, e^{i\Delta\omega t} \cdot \mathrm{Tr}_a \{\boldsymbol{d}\cdot\boldsymbol{d}\langle U(t)\rangle_p\}\,. \tag{2.1}$$

$\Delta\omega$ is the frequency distance from the frequency of the unperturbed line, $\boldsymbol{d}$ is the operator of the atomic dipole moment, Tr_a extends over the states of the upper level involved in the transition, and $U(t)$ is the evolution operator satisfying the Schrödinger equation

$$i\hbar\dot{U}(t) = -\boldsymbol{d}\cdot\boldsymbol{E}(t)\,U(t)\,, \quad U(0)=1\,, \tag{2.2}$$

in an interaction picture where the unperturbed oscillations have been split off. The electric microfield $\boldsymbol{E}(t)$ has to be taken at the atomic position at time t, and $\langle\ldots\rangle_p$ denotes an average over initial perturber positions and velocities or, equivalently, over all possible realizations of $\boldsymbol{E}(t)$.

(2.1) is the standard starting point for Stark broadening calculations, and I shall mention just one of the assumptions necessary for its derivation: The radiating atom is taken to be at rest. By this, Stark broadening becomes independent of the atomic thermal velocity and any correlation of Stark and Doppler broadening is neglected. This approximation is well justified for electron perturbers, but it cannot be readily accepted whenever ion dynamical effects have an influence on the line profile [30]. Nevertheless, as it is a difficult task of its own to take account of the dependence of Stark broadening on the emitter velocity, I shall adopt the common procedure to get rid of this problem: To compensate roughly for the neglect of radiator motion, the true ion perturbers are replaced by fictious ones with the reduced mass μ of the radiating atom — true ion pair.

With the real plasma microfield in (2.2) it is impossible to find the exact line profile or the exact mean evolution operator which is the key quantity in (2.1). Therefore, it is common practice to try to calculate an approximate line profile for the true microfield at least in principle. (Actual calculations often use an approximate microfield as well [31].) Contrary to this, Brissaud and Frisch [23] have proposed to proceed the other way: To calculate

the exact line profile for an approximate microfield, the "model microfield".

2.2. General form of the MMM

The most general model microfield for which the mean evolution operator has been evaluated [24, 28, 29] consists of the set of all step functions

$$\boldsymbol{E}(t) = \begin{cases} \boldsymbol{E}_0, & 0 \leqq t < t_0, \\ \boldsymbol{E}_1, & t_0 \leqq t < t_1 \\ \boldsymbol{E}_2, & t_1 \leqq t < t_2 \\ \cdot & \\ \cdot & \\ \cdot & \end{cases} \tag{2.3}$$

with field strength probability densities $P(\boldsymbol{E}_0)$ and $Q(\boldsymbol{E}_1)$, $Q(\boldsymbol{E}_2), \ldots$ and probability density functions $w(t_0 \mid \boldsymbol{E}_0)$, $v(t_1 - t_0 \mid \boldsymbol{E}_1)$, $v(t_2 - t_1 \mid \boldsymbol{E}_2), \ldots$ for the duration of $\boldsymbol{E}_0$, $\boldsymbol{E}_1$, $\boldsymbol{E}_2, \ldots$. The vector-valued stochastic process defined in this way is stationary if

$$\begin{aligned} Q(\boldsymbol{E}) &= w(0 \mid \boldsymbol{E})\, P(\boldsymbol{E}) / \langle w(0 \mid \boldsymbol{E}) \rangle_{\mathrm{s}} \quad \text{and} \\ v(t \mid \boldsymbol{E}) &= -\dot{w}(t \mid \boldsymbol{E}) / w(0 \mid \boldsymbol{E}) \end{aligned} \tag{2.4}$$

hold; the "static average" $\langle \ldots \rangle_{\mathrm{s}}$ is taken according to $P(\boldsymbol{E})$. As the process loses all memory of its previous state whenever $\boldsymbol{E}(t)$ jumps to a new value, it has been termed a "renewal (or recurrent) process (RP)" [28, 29]. It should be clear from this definition that all statistical properties of a stationary RP are fixed by P and w. (In what follows, stationarity will always be tacitly presupposed.)

With a stationary renewal process as coefficient in the right hand side of (2.2), the Laplace transform of the mean evolution operator is

$$\begin{aligned} \langle \tilde{U}(\omega) \rangle_{\mathrm{RP}} &= \left\langle \int_0^\infty \mathrm{d}t\, e^{i\omega t}\, U(t) \right\rangle_{\mathrm{RP}} \\ &= \int_0^\infty \mathrm{d}t\, e^{i\omega t} \left\langle \int_t^\infty \mathrm{d}s\, w(s \mid \boldsymbol{E})\, U(t \mid \boldsymbol{E}) \right\rangle_{\mathrm{s}} \\ &\quad + \left[\int_0^\infty \mathrm{d}t\, e^{i\omega t} \langle w(t \mid \boldsymbol{E})\, U(t \mid \boldsymbol{E}) \rangle_{\mathrm{s}} \right] \\ &\quad \cdot \left[\langle w(0 \mid \boldsymbol{E}) \rangle_{\mathrm{s}} + \int_0^\infty \mathrm{d}t\, e^{i\omega t} \langle \dot{w}(t \mid \boldsymbol{E})\, U(t \mid \boldsymbol{E}) \rangle_{\mathrm{s}} \right]^{-1} \\ &\quad \cdot \left[\int_0^\infty \mathrm{d}t\, e^{i\omega t} \langle w(t \mid \boldsymbol{E})\, U(t \mid \boldsymbol{E}) \rangle_{\mathrm{s}} \right]; \end{aligned} \tag{2.5}$$

according to (2.1), its real part is needed to calculate the line profile. (In (2.5), $U(t \mid \boldsymbol{E}) = \exp(i\boldsymbol{d} \cdot \boldsymbol{E} t/\hbar)$ is the evolution operator in a static field $\boldsymbol{E}$.) In order to get a line profile from (2.5) which approximates the true profile, the functions P and w have to reflect the main statistical features of the plasma microfield. Clearly, P must be the true microfield probability density to obtain the correct "static wing" from (2.5). The present work will be confined to isotropic plasmas, hence one may set

$$P(\boldsymbol{E}) = (4\pi E^2)^{-1} P(E) \tag{2.6}$$

and $w(t \mid \boldsymbol{E}) = w(t \mid E)$. Then, the autocorrelation function of the model microfield is

$$\begin{aligned} \Gamma_{\mathrm{RP}}(t) &= \langle \boldsymbol{E}(0) \cdot \boldsymbol{E}(t) \rangle_{\mathrm{RP}} \\ &= \int_0^\infty \mathrm{d}E\, E^2\, P(E) \int_t^\infty \mathrm{d}s\, w(s \mid E), \end{aligned} \tag{2.7}$$

and w should be chosen in such a way as to reproduce the true microfield correlation:

$$\Gamma_{\mathrm{RP}}(t) = \Gamma(t) = \langle \boldsymbol{E}(0) \cdot \boldsymbol{E}(t) \rangle_p,$$

which determines the line core in the impact limit [23, 28, 32]. (At this point the assumption that the radiator is at rest plays an important role: For a radiator moving with constant velocity the plasma would appear to be anisotropic, and the correlation tensor $\langle \boldsymbol{E}(0) \otimes \boldsymbol{E}(t) \rangle_p$ should be used instead of $\Gamma(t)$ [30].) Though this requirement does not fix $w(t \mid E)$ in general, it is sufficient for the two special renewal processes to be discussed next.

Before this is done, I should like to call attention to another two points. The first concerns the possible types of w and Γ_{RP}. v in (2.4) is a probability density, i.e. non-negative, and so is w. Hence, $w(t \mid E)$ may never increase with increasing t, and Γ_{RP} must be non-negative, too. Secondly, the generalization of the MMM should be mentioned which consists of the superposition of a slow and a fast RP corresponding to the low and high frequency components of the plasma microfield [23, 28]. In that case, (2.5) has to be used twice: One starts with the calculation of the electronic mean of the evolution operator for constant ionic fields, and then inserts this instead of $U(t)$ into (2.5) where the averages relate to ionic fields now. In general, this brings about an additional difficulty as the first step yields the Laplace transform $\langle \tilde{U}(\omega \mid \boldsymbol{E}_i) \rangle_{\mathrm{e}}$, not the evolution operator itself.

2.3. Kangaroo process

The original presentation of the MMM by Brissaud and Frisch [23] as well as all line broadening calculations effected with its help later on [17, 25,

26, 28] have used a special renewal process, the "kangaroo process (KP)". It is defined to be the Markovian renewal process which loses all memory of its previous state not only when a jump occurs to a new value of the field strength, but instantaneously at every time. Accordingly, w and v have to be equal to one another for a KP. This provides a simple differential equation for w, the normalized solution of which is

$$w(t|E) = \Omega(E)\exp[-\Omega(E)t]. \tag{2.8}$$

The autocorrelation function of the model microfield becomes, for a KP,

$$\Gamma_{\mathrm{KP}}(t) = \int_0^\infty \mathrm{d}E\, E^2\, P(E)\exp[-\Omega(E)t]. \tag{2.9}$$

Under the reasonable assumption that Ω is strictly increasing to infinity with increasing E, the right hand side of (2.9) is essentially a Laplace transform and, given $\Gamma_{\mathrm{KP}} = \Gamma$, the dependence of Ω on E can be calculated after inverting this Laplace transform and solving a simple differential equation [23, 24]. Once $\Omega(E)$ and $P(E)$ are known, the KP line profile follows from

$$\begin{aligned}&\langle \tilde{U}(\omega)\rangle_{\mathrm{KP}}\\ &= \langle \tilde{U}(\omega'|\boldsymbol{E})\rangle_{\mathrm{s}} + \langle \Omega(E)\,\tilde{U}(\omega'|\boldsymbol{E})\rangle_{\mathrm{s}}\\ &\quad\cdot[\langle\Omega(E)\rangle_{\mathrm{s}} - \langle\Omega^2(E)\,\tilde{U}(\omega'|\boldsymbol{E})\rangle_{\mathrm{s}}]^{-1}\\ &\quad\cdot\langle\Omega(E)\,\tilde{U}(\omega'|\boldsymbol{E})\rangle_{\mathrm{s}},\end{aligned} \tag{2.10}$$

with the Laplace transform of $U(t|\boldsymbol{E})$ taken at $\omega' = \omega + i\Omega(E)$.

2.4. *Theta process*

For the KP, every instant of time is a renewal point, it has no memory at all. In contrast to this, the renewal process with.

$$\begin{aligned}w(t|E) &= \theta[T(E) - t]/T(E),\\ v(t|E) &= \delta[t - T(E)]\end{aligned} \tag{2.11}$$

has the most persistent memory a renewal process may have: If a jump at time t leads to a field strength $\boldsymbol{E}$, the next jump will happen at precisely $t + T(E)$, i.e., every field strength has a definite life span $T(E)$. Because of the θ-(step-)function in (2.11) I shall refer to this process shortly as the "theta process (TP)".

The autocorrelation function for the TP is

$$\begin{aligned}\Gamma_{\mathrm{TP}}(t) = \int_0^\infty \mathrm{d}E\, E^2\, P(E)\\ \cdot[1 - t/T(E)]\,\theta[T(E) - t].\end{aligned} \tag{2.12}$$

Provided that $T(E)$ decreases continuously with increasing E to $T(E=\infty)=0$, it is easily shown that

$$\begin{aligned}&\Gamma_{\mathrm{TP}}[T(E)] - T(E)\,\dot{\Gamma}_{\mathrm{TP}}[T(E)]\\ &= \int_0^E \mathrm{d}F\, F^2\, P(F)\end{aligned} \tag{2.13}$$

must hold. If $\Gamma_{\mathrm{TP}} = \Gamma$ is prescribed, solving (2.13) for $T(E)$ furnishes the life spans of the different field strengths. For the mean TP evolution operator insertion of (2.11) into (2.5) has the result

$$\begin{aligned}\langle\tilde{U}(\omega)\rangle_{\mathrm{TP}} &= \left\langle \int_0^T \mathrm{d}t\, e^{i\omega t}\left(1 - \frac{t}{T}\right) U(t|\boldsymbol{E})\right\rangle_{\mathrm{s}}\\ &\quad + \left\langle \frac{1}{T}\int_0^T \mathrm{d}t\, e^{i\omega t}\, U(t|\boldsymbol{E})\right\rangle_{\mathrm{s}}\\ &\quad\cdot\left\langle \frac{1}{T}\,[1 - e^{i\omega T}\, U(T|\boldsymbol{E})]\right\rangle_{\mathrm{s}}^{-1}\\ &\quad\cdot\left\langle \frac{1}{T}\int_0^T \mathrm{d}t\, e^{i\omega t}\, U(t|\boldsymbol{E})\right\rangle_{\mathrm{s}}.\end{aligned} \tag{2.14}$$

(T is $T(E)$ here.)

2.5. *Comparison of KP and TP*

Even if a KP and a TP have the same probability density P for the field strengths and identical autocorrelation functions, $\Gamma_{\mathrm{KP}} = \Gamma_{\mathrm{TP}} = \Gamma$, they are quite different as for more subtle statistical properties. The mean duration of an initial field $\boldsymbol{E}$, for example, is $1/\Omega(E)$ for the KP and $T(E)/2$ for the TP, and in general these two values differ as a comparison of (2.9) and (2.12) shows. Even if they are the same for some field E, the relaxation from this initial field takes place in different ways. To illustrate this, Fig. 1 displays the "conditional covariance"

$$\begin{aligned}&\gamma(t|E)\\ &= \int \mathrm{d}^3F\, \boldsymbol{F}\cdot\boldsymbol{E}\, P_2(\boldsymbol{F},t;\boldsymbol{E},0)/P(\boldsymbol{E})\end{aligned} \tag{2.15}$$

for $T(E) = 2/\Omega(E)$. As

$$\begin{aligned}\gamma_{\mathrm{KP}}(t|E) &= E^2\exp[-\Omega(E)t] \quad\text{and}\\ \gamma_{\mathrm{TP}}(t|E) &= E^2[1 - t/T(E)]\,\theta[T(E) - t]\end{aligned}$$

are rather different functions regardless of what values are chosen for Ω and T, it is clear that the two-time probability density $P_2(\boldsymbol{F},t;\boldsymbol{E},0)$ is not the same for a KP and a TP. (Note, however, that the mere fact that KP and TP have been construct-

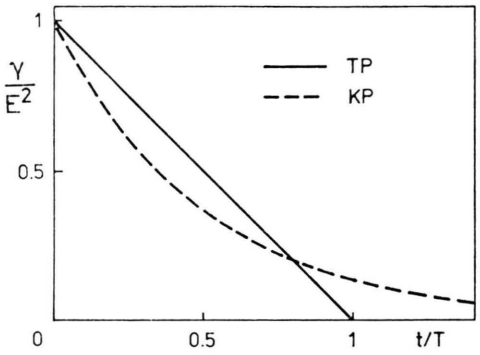

Fig. 1. "Conditional covariances" $\gamma_{\mathrm{KP}}=E^2\exp(-\Omega t)$ (broken line) and $\gamma_{\mathrm{TP}}=E^2\,(1-t/T)\,\theta(T-t)$ (full line) with $T=2/\Omega$.

ed as proper stochastic processes guarantees the correct short and long time behaviour of P_2: $P_2(\boldsymbol{F},0;\,\boldsymbol{E},0)=\delta(\boldsymbol{F}-\boldsymbol{E})$, $P(E)$, $P_2(\boldsymbol{F},\infty;\boldsymbol{E},0)=P(\boldsymbol{F})\,P(\boldsymbol{E})$.) Hence, if any part of a line profile is sensitive to the exact form of P_2 or any higher order probability density, marked deviations of the TP from the KP line profile should show up.

Two other differences relate to the numerical realization of MMM calculations. As opposed to the rather complicated way the jumping frequencies $\Omega(E)$ have to be calculated from $\Gamma(t)$ for a KP, the life spans $T(E)$ for a TP are easily obtained as solutions of (2.13). On the other hand, use of the KP is more advantageous if a superposition of an electronic and an ionic microfield is to be processed: According to (2.10), the KP calculation can be done entirely with the Laplace transform of the evolution operator while the TP calculation is more involved.

3. Lyman Line Profiles

3.1. General results

The trace in (2.1) is most conveniently evaluated in angular momentum eigenstates $|nlm\rangle$:

$$I(\Delta\omega)\propto\mathrm{Re}\int_0^\infty \mathrm{d}t\,e^{i\Delta\omega t}\cdot\sum_{\substack{l,m\\ l',m'}}\langle nlm|\,\boldsymbol{d}\,|100\rangle\cdot\langle 100|\,\boldsymbol{d}\,|nl'm'\rangle\cdot\langle nl'm'|\,\langle U(t)\rangle_p\,|nlm\rangle \tag{3.1}$$

for the Lyman line with principal quantum number n of the upper level. (By the "no quenching approximation", $U(t)$ is restricted to work in $\mathfrak{H}_n$ only, the space of atomic states with just this principal quantum number.) As a result of the selection rules for the components of the atomic dipole moment [33], knowledge of three diagonal elements of $\langle U(t)\rangle_p$ is sufficient:

$$I(\Delta\omega)\propto\mathrm{Re}\int_0^\infty \mathrm{d}t\,e^{i\Delta\omega t}\cdot\sum_{m=-1}^{1}\langle n1m|\,\langle U(t)\rangle_p\,|n1m\rangle\propto\mathrm{Re}\sum_{m=-1}^{1}\langle n1m|\,\langle\tilde{U}(\Delta\omega)\rangle_p\,|n1m\rangle. \tag{3.2}$$

For an isotropic renewal process, the angular part of the static average

$$\langle\ldots\rangle_{\mathrm{s}}=\int_0^\infty \mathrm{d}E\,E^2P(E)\,\frac{1}{2}\int_0^\pi \mathrm{d}\vartheta\sin\vartheta\,\frac{1}{2\pi}\int_0^{2\pi}\mathrm{d}\varphi\ldots$$

in (2.5) relates to $U(t\,|\,\boldsymbol{E})=\exp(i\boldsymbol{d}\cdot\boldsymbol{E}t/\hbar)$ only (ϑ and φ are polar angles of $\boldsymbol{E}$). But

$$e^{i\boldsymbol{d}\cdot\boldsymbol{E}t/\hbar}=e^{-i\varphi l_z/\hbar}\,e^{-i\vartheta l_y/\hbar}\,e^{id_zEt/\hbar}\cdot e^{i\vartheta l_y/\hbar}\,e^{i\varphi l_z/\hbar}, \tag{3.3}$$

and as d_z is diagonal in the magnetic quantum number m, so is $\exp(id_zEt/\hbar)$. With this in mind, it is not difficult to prove that the angular average reduces $\exp(i\boldsymbol{d}\cdot\boldsymbol{E}t/\hbar)$ to diagonal form:

$$\langle nlm|\,\langle e^{i\boldsymbol{d}\cdot\boldsymbol{E}t/\hbar}\rangle_{\varphi,\vartheta}\,|nl'm'\rangle=\frac{\delta_{ll'}\,\delta_{mm'}}{2l+1}\sum_{\mu}\langle nl\mu|\,e^{id_zEt/\hbar}\,|nl\mu\rangle, \tag{3.4}$$

the diagonal elements being independent of m.

From the theory of the linear Stark effect of hydrogen it is well known [33] that d_z (restricted to $\mathfrak{H}_n$) has eigenvalues $\frac{3}{2}nkea_0$, $k=1-n,\,2-n,\ldots,n-1$. Therefore, the sum in (3.4) is

$$\sum_{\mu}\langle nl\mu|\,e^{id_zEt/\hbar}\,|nl\mu\rangle=\sum_{k=1-n}^{n-1}\alpha'_{kl}\,e^{i\frac{3}{2}nkea_0Et/\hbar} \tag{3.5}$$

with constant coefficients α'_{kl}. With diagonal $\langle U(t\,|\,\boldsymbol{E})\rangle_{\mathrm{s}}$, $\langle\tilde{U}(\omega)\rangle_{\mathrm{RP}}$ is diagonal, too, and according to (3.2) it is sufficient to know the matrix elements $\langle n1m|\,\langle U(t\,|\,\boldsymbol{E})\rangle_{\mathrm{s}}\,|n1m\rangle$, i.e., the coefficients $\alpha'_k=\alpha'_{k1}$. Their meaning becomes clear if broadening by static fields $\boldsymbol{E}$ is examined, which have fixed modulus E but random directions. In that case, $\langle\exp(i\boldsymbol{d}\cdot\boldsymbol{E}t/\hbar)\rangle_{\vartheta,\varphi}$ is the full mean evo-

lution operator, and insertion of (3.4) and (3.5) into (3.2) has to produce the usual static Stark profile

$$I(\Delta\omega) \propto \sum_{k=1-n}^{n-1} \alpha_k' \, \delta(\Delta\omega + \tfrac{3}{2} n k e a_0 E/\hbar). \quad (3.6)$$

This shows that the α_k' give the relative intensities of the static Stark components of the Lyman line under consideration (for example, $\alpha_{-1}' : \alpha_0' : \alpha_1' = 1:4:1$ for L_α). Moreover, setting $t=0$ in (3.5) yields $\sum_k \alpha_{kl}' = 2l+1$ and especially $\sum_k \alpha_k' = 3$.

With the definitions $\alpha_k = \alpha_k'/3$ and $\tilde{w}(\omega|E) = \int_0^\infty \mathrm{d}t \, w(t|E) \exp(i\omega t)$, insertion of all this into (2.5) results in

$$\begin{aligned} &- i\langle n1m | \langle \tilde{U}(\omega)\rangle_{\mathrm{RP}} | n1m\rangle \\ &= \sum_k \alpha_k \left\langle \frac{1-\tilde{w}(\Delta\omega_k|E)}{\Delta\omega_k} \right\rangle_E \\ &+ \left\{ \sum_k \alpha_k \langle \tilde{w}(\Delta\omega_k|E)\rangle_E \right\}^2 \\ &\cdot \left\{ \sum_k \alpha_k \langle \Delta\omega_k \tilde{w}(\Delta\omega_k|E)\rangle_E \right\}^{-1} \end{aligned} \quad (3.7)$$

for Lyman line broadening by renewal processes. $\Delta\omega_k$ is an abbreviation for $\Delta\omega + \frac{3}{2} n k e a_0 E/\hbar$ and $\langle \ldots \rangle_E$ stands for $\int_0^\infty \mathrm{d}E \, P(E) \ldots$ in (3.7). Normalized to total intensity π, the RP profile is the negative imaginary part of the right hand side of (3.7).

3.2. KP profiles

For the KP, the Laplace transform of $w(t|E)$ is

$$\tilde{w}(\Delta\omega_k|E) = \frac{\Omega}{\Omega - i\Delta\omega_k} = \Omega \frac{\Omega + i\Delta\omega_k}{\Omega^2 + (\Delta\omega_k)^2}. \quad (3.8)$$

According to (3.7), this quantity as well as

$$\Delta\omega_k \cdot \tilde{w}(\Delta\omega_k|E) \quad \text{and}$$
$$-\mathrm{Im}(1-\tilde{w})/\Delta\omega_k = \Omega/[(\Delta\omega_k)^2 + \Omega^2]$$

have to be averaged with respect to E (both $\Delta\omega_k$ and Ω depend on E!). It is not difficult to do this approximately with a computer.

3.3. TP profiles

The Laplace transform of w for the TP is conveniently written as

$$\tilde{w}(\Delta\omega_k|E) = \frac{2}{\Delta\omega_k T} \sin\frac{\Delta\omega_k T}{2} \exp\left(i\frac{\Delta\omega_k T}{2}\right), \quad (3.9)$$

from which one has

$$-\mathrm{Im}(1-\tilde{w})/\Delta\omega_k = \frac{2}{(\Delta\omega_k)^2 T} \sin^2\frac{\Delta\omega_k T}{2}.$$

Because of the trigonometric functions, the numerical evaluation of the E-average is more involved than for the KP, and some care has to be taken to obtain correct contributions from both small and large values of $\Delta\omega_k T/2$.

4. Numerical Results

4.1. General considerations

KP and TP line profiles have been obtained by numerically evaluating (3.7) after insertion of (3.8) or (3.9), respectively, for the first four Lyman lines L_α to L_δ (i.e., $n=2, 3, 4, 5$) broadened by either electrons or ions alone. The computations have been done for a plasma temperature of 10^4 K and electron (or ion) densities from 10^{15} to 10^{17} cm^{-3} — values which are about typical for laboratory plasmas produced in a stationary arc, say. Under these conditions, it is impossible to observe ion and electron broadening separately, hence none of the profiles shown here is realistic (quite apart from the fact that Doppler broadening is neglected). However, differences in the line profiles brought about by the use of the TP instead of the KP in the MMM will become more conspicious if ion and electron broadening are isolated from one another in the calculations.

The microfield probability densities and autocorrelation functions used in the computations are those for a plasma of non-interacting statically screened ions and electrons; former work with the KP version of the MMM [17, 28] has demonstrated that they yield realistic line profiles. The screening length is taken to be twice the Debye length for electrons, $R_e = 2D = [kT/(\pi N e^2)]^{1/2}$, and $R_i = [kT/(5\pi N e^2)]^{1/2}$ for ions. This choice leads to microfield distributions in close agreement with those given by Baranger and Mozer [34, 35] or Hooper [36, 37]. (In fact, the tabulation of the Baranger-Mozer results given by Pfennig and Trefftz [38] has been employed for the static averages in (3.7).) The microfield autocorrelation function $\Gamma(t)$ for an ideal gas of statically screened charged particles is known in closed form [32], and the equation from which the jumping frequencies of the KP have to be de-

termined has been obtained previously [28], too. On the other hand, it is not difficult to solve (2.13) for the life spans of the TP fields if an analytical expression is known for $\Gamma_{TP}=\Gamma$. Therefore, the computation of KP as well as TP profiles from (3.7) does not pose too hard numerical problems.

Yet there is a problem: the duration of weak fields. $\Gamma(t)$ decreases asymptotically as t^{-5} for the plasma model described above, and from (2.9) and (2.12) it is obvious that KP and TP must have $\Omega\to 0$ and $T\to\infty$ for vanishing E to reproduce this slow decay. Therefore, weak model microfields last very long times and may even produce static line broadening. A closer inspection of the appropriate limit reveals that this does not arise for electron broadening, but it does concern ion broadening in the density range considered here, especially for the TP. As a result, rather unusual features appear in the very line centres; the profile of L_β, for example, broadened by ions only, exhibits a tiny bump in the middle of the deep central depression. Of course, such structures would not be found in the full line profiles as they are smeared out by electron as well as Doppler broadening. Moreover, weak fields are not expected to last forever in reality — as they are due to many pertubers, their life time cannot be much longer than the inverse of the corresponding plasma frequency. To take account of this, the model microfields have been modified by introducing a lower cutoff at w_p for the KP jumping frequency Ω and an upper cutoff at ω_p^{-1} for the TP life span T. ($\omega_p=(4\pi Ne^2/m)^{1/2}$ is the plasma frequency, with $m=m_e$ for electrons and $m=\mu$, the reduced atom-ion mass, for ions.) As to Γ_{KP} and Γ_{TP}, this measure results in an alteration of the long time behaviour which does not affect the line profiles except by suppressing static contributions of weak fields. At this point, a general remark on the validity of the MMM seems to be appropriate. It should be clear from what has just been discussed that the reproduction of the true autocorrelation function $\Gamma(t)$ by the model microfield does not automatically guarantee that weak and strong model fields have the correct duration — this may or may not be the case depending on the probability density $w(t|E)$. For that reason, the additional freedom provided by the choice of this function in the general RP version of the MMM may be valuable. In the problem considered here, for example, no cutoff would be necessary for $w(t|E)=w[t/\tau(E)]$ with $w\propto[\tau(E)/t]^6$ at $t\to\infty$, as one might choose $\tau(0)$ finite then. Unfortunately, no functional form of w complying with this condition has been found which allows for a simple determination of $\tau(E)$ from $\Gamma(t)$.

Contrary to weak fields, strong fields must lead to nearly static line broadening. The average life time of strong KP fields is known [28] to be proportional to $E^{-1/2}$, and it turns out that the same is true for strong TP fields. Accordingly, KP as well as TP profiles have the correct static line wings; this will be demonstrated at once by the results to be shown now.

4.2. Broadening by electrons

Under the influence of electron broadening only, the Lyman line profiles should have a Lorentzian impact core out to $|\Delta\omega|\cong\omega_{pe}$ and static Holtsmark wings with the characteristic $|\Delta\omega|^{-5/2}$-decrease for $|\Delta\omega|\gg\omega_{pe}$. Both KP and TP profiles show these features for all lines at all densities which have been investigated. Figure 2 gives a typical example, L_γ at $N=10^{16}$ cm^{-3}, which illustrates the transition from impact to static broadening. For the purpose of comparison, the static profile has been inserted

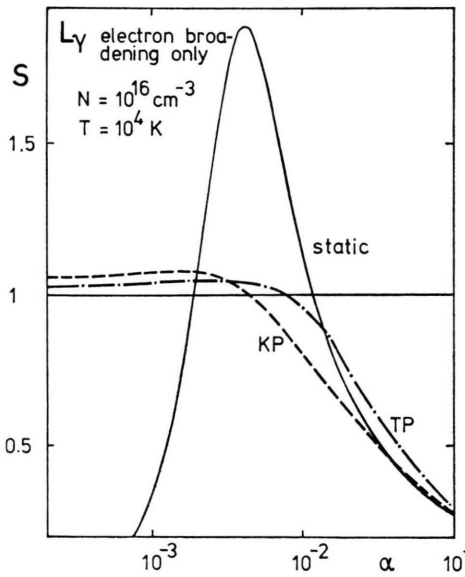

Fig. 2. KP and TP profiles of L_γ broadened by electrons with density 10^{16} cm^{-3} and temperature 10^4 K. The representation is relative to the impact profile, and the static profile has been inserted as well to demonstrate the smooth transition of MMM profiles from the impact core to the static line wing. (α is the usual reduced wavelength distance from the line centre [2, 11]. The ordinate should have been designated S/S_{impact} rather than S.)

as well. To make the figure more lucid, all profiles are given relative to the impact profile which corresponds to impact parameter cutoffs at $\varrho_{\min} = n^2\hbar/(m_e v)$ and $\varrho_{\max} = D$ (Debye length), and a Lorentz-Weisskopf treatment of strong collisions. There are small differences between the MMM profiles and the impact profile in the line centre, but these are most probably due to the different treatment of strong collisions.

By the example given it may be judged that the general agreement of KP and TP profiles is remarkably good over the full intensity range. (Note that the impact profile used in Fig. 2 changes by more than three decades there, from 217 at $\alpha = 10^{-4}$ to 0.046 at $\alpha = 10^{-1}$!) However, a detailed investigation of the differences between the two profiles reveals systematic deviations of the TP profile from the KP profile (or vice versa): The TP intensity is always slightly lower in the line centre than the KP intensity (from 0.2% for L_α at 10^{16} cm^{-3} to 6.1% for L_δ at 10^{17} cm^{-3}), but it becomes about 20% higher at $\Delta\omega \cong 3\omega_{pe}$. Further out in the line wing, both profiles merge again as they become more and more static. In Fig. 3, the relative deviation of the TP from the KP intensity is shown for the profiles of Figure 2. Most pronounced differences are found in the transition region around that value of α where the impact and static line wings intersect. This happens at about $3\alpha_{pe}$, where α_{pe} corresponds to a frequency distance from the line centre which is equal to the plasma frequency (for electrons, in this case).

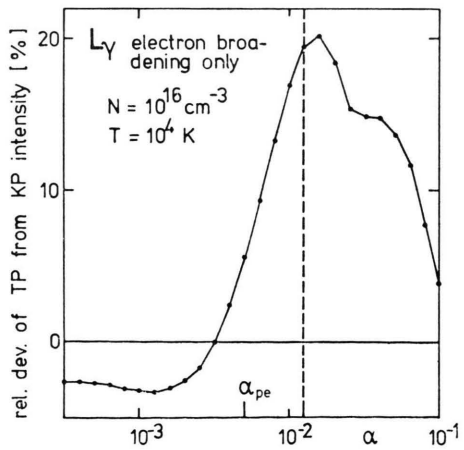

Fig. 3. Relative deviation of the TP from the KP profile of Figure 2. $\alpha_{pe} \cong 5 \cdot 10^{-3}$ corresponds to $\Delta\omega = \omega_{pe}$, and the broken vertical line marks that value of α where the impact profile intersects the wing of the static profile (cf. Figure 2). Marked deviations are found only in the transition region between the impact core ($\alpha \lesssim \alpha_{pe}$) and the static wing ($\alpha \gtrsim 10^{-1}$ here, just out of scale).

Nearly the same deviations of up to 20% at $\alpha \cong 3\alpha_{pe}$ have been found for all other lines and densities, too. Evidently, these deviations stem from the different higher order statistical properties of the two model microfields. (It has been tested that the cutoffs which have been imposed on Ω and T do not have a noticeable influence on the transition region.) Accordingly, similar errors have to be expected in that part of the MMM profiles as compared to the true line profiles. It should be born in mind, however, that these errors are reduced by the additional ion and Doppler broadening which have been neglected here.

4.3. Broadening by ions

Contrary to electron broadening, broadening by ions is not impact broadening in the line centre for the densities and temperature considered here. Therefore, the corresponding line profiles have static wings (for $|\Delta\omega| \gg \omega_{pi}; \omega_{pi}$ is the ionic plasma frequency now, computed with the reduced atom-ion mass) but the whole line core belongs to the "transition region" where the MMM presumably works least reliable.

All ion broadening calculations have been done for the atom-ion pair H-Ar$^+$. Figures 4 and 5 give two typical examples for the KP and TP profiles which have been obtained. Figure 4 shows a line with central depression, L_β at $N = 10^{16}$ cm^{-3}, while Fig. 5 presents a line with central maximum, L_γ at the same density. (With electron broadening, this distinction was not necessary as Lorentzian impact cores always have a central maximum.) Again the general agreement of KP and TP profiles is good for all values of α, and both possess the correct static wing. But there are differences in the line cores, out to approximately $10\alpha_{pi}$ where eventually both profiles nearly coincide with the static one.

The relative deviations are depicted in Fig. 6 and 7 for these two lines; they are characteristic examples of all results for ion broadening. Generally speaking, the differences indicate a more "static" action of TP fields as TP profiles have somewhat more pronounced structures than KP profiles. Just as in the case of electron broadening, relative deviations reach about 20% and may be found especially around $3\alpha_{pi}$. (Less pronounced deviations in

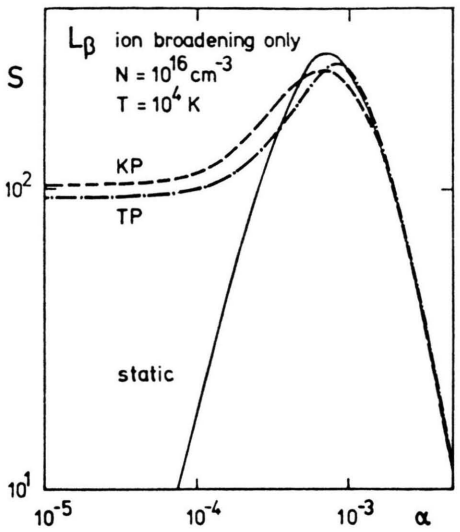

Fig. 4. KP and TP profiles of L_β, a line without central component in static fields, broadened by Ar^+-ions with density 10^{16} cm^{-3} and temperature 10^4 K. In the line wing, both profiles coincide with the static profile which is shown as well. For the line core, no simple approximation is known for ion broadening. (All $S(\alpha)$ are normalized to unit total area.)

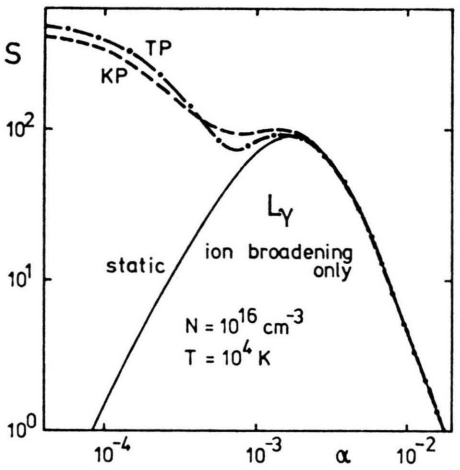

Fig. 5. Same as Fig. 4, but for L_γ which has a strong central component in static fields.

the opposite direction show up near the location of the intensity maximum to maintain area normalization.) Altogether, the situation is very much the same as with electron broadening, and so are the errors which may be brought about by the use of the MMM.

In a strict sense, the differences between KP and TP profiles found here do not allow a conclusion with regard to the deviations of MMM from true line profiles because the true microfield is neither a KP nor a TP. Still, these differences give for the first time a quantitative estimate of the influence which higher order statistical features of the microfield exert on hydrogen line profiles. In this connexion, it is interesting to note that the errors of MMM-KP profiles (including both electron and ion broadening) as compared to experimental results amount to about 10 to 20% as well. According to the results presented here, this may well be due to the use of the special KP form of $w(t \mid E)$.

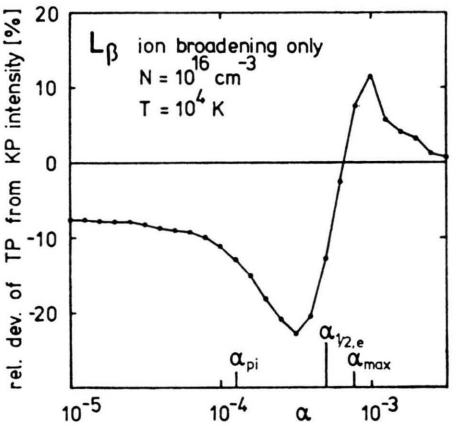

Fig. 6. Relative deviation of the TP from the KP profile of Fig. 4 (L_β). $\alpha_{pi} \cong 1.3 \cdot 10^{-4}$ corresponds to $\Delta\omega = \omega_{pi}$, where the plasma frequency has been calculated with the reduced mass of the atom-ion pair H-Ar^+ (i.e., practically the atomic mass). α_{max} denotes the approximate position of the intensity maximum, and $\alpha_{1/2,e}$ is the half width effected by electron broadening only.

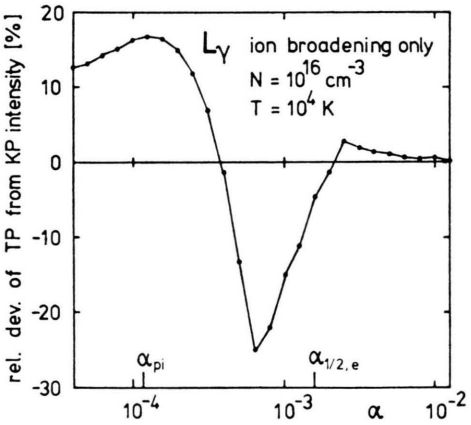

Fig. 7. Same as Fig. 6, but for the L_γ profiles of Figure 5. For L_γ, the intensity has its maximum in the line centre, $\alpha = 0$.

5. Summary and Conclusions

To test the reliability of the "model microfield method (MMM)" two different model microfields have been used to calculate Stark profiles of hydrogen resonance lines broadened by ions or electrons. One of these, the Markovian "kangaroo process (KP)" has been applied in all previous computations of MMM profiles as well as in the original presentation of the method [17, 23, 25, 26, 28]. The other one, a special non-Markovian renewal process, has been defined in Sect. 2.4 and shortly termed "theta process (TP)". If their parameters are suitably chosen, the KP and TP model microfields coincide with one another and with the true plasma microfield as to the probability density $P(E)$ and the autocorrelation function $\Gamma(t) = \langle \boldsymbol{E}(t) \cdot \boldsymbol{E}(0) \rangle$, but all the three differ with respect to higher order statistical properties. The MMM is based on the fundamental assumption that line profiles are determined essentially by just P and Γ; a comparison of KP and TP profiles allows to test this assumption and to estimate the influence of more complicated statistical details.

Line profiles have been calculated for the Lyman lines L_α to L_δ broadened by either electrons or ions with a temperature of 10^4 K and densities ranging from 10^{15} cm^{-3} to 10^{17} cm^{-3}. For electron broadening, it is well known that P and Γ determine the line wing and core, respectively [2]. Indeed, KP and TP profiles show marked deviations only in the transition region in between which increase up to about 20% at a frequency separation from the line centre of approximately three times the electron plasma frequency. These figures are nearly the same for all lines and densities investigated. For ion broadening, too, the static line wing is given by P. However, no simple description of the line core is known, and errors brought about by the use of the MMM should be found in this part of the profile. (There is another difference between electron and ion broadening: Strictly, radiator motion cannot be neglected as compared to ion motion [30]. To account for this at least approximately, the ionic mass has been taken to be the reduced atom-ion mass here.) Once more, the most pronounced differences of KP and TP profiles show up at a frequency separation of the order of three times the (ion) plasma frequency, and again they amount to about 20% there as in the case of electron broadening.

For the full line profiles, the simultaneous action of electrons and ions would have to be considered (together with the additional Doppler broadening). The computations are much more involved then even for Lyman lines, and have not been tackled for this reason. Yet it seems to be clear that the superposition of electron and ion broadening will result in a reduction of the differences between KP and TP profiles as it is roughly similar to a convolution of the corresponding profiles given here, especially for L_α. But even a reduction by a factor 1/2 would leave uncertainties of the order of 10% which are inherent in the MMM and set a fundamental limit to its accuracy — the point is that there is no criterion to decide which one of the two model microfields (or any other renewal process) should be chosen as long as the correct reproduction of P and Γ is all that is required. Then, indeed, a convenient functional form of $w(t|E)$ may be prescribed a priori as it has always been done up to now.

The results presented here, however, show that the choice of w has to be done carefully as it does affect noticeably those portions of the line profiles which are not determined by P or Γ alone. But which w is best ? A hint to the answer of this question may have been given by the discussion concerning the duration of weak fields in Section 4.1. There it has been shown that some w lead to unrealistic features of the model microfield if $\int_t^\infty \mathrm{d}s\, w(s|E)$ is not well suited for the reproduction of $\Gamma(t)$ with respect to the long time tail, for example. Hence, it seems to be most appropriate to start with the general RP version of the MMM (Sect. 2.2) and to choose $\int_t^\infty \mathrm{d}s\, w(s|E)$ to be the normalized "conditional covariance"

$$E^{-2}\gamma(t|E) = E^{-2}\int \mathrm{d}^3F\, \boldsymbol{F}\cdot\boldsymbol{E}\, P_2(\boldsymbol{F},t;\boldsymbol{E},0)/P(\boldsymbol{E})$$

of the true microfield. According to (2.7), this implies the correct autocorrelation function as well, but — in addition — this special RP model microfield would take proper account of the relaxation of every initial field-strength E. By this, it would be most perfectly adjusted to the true microfield and might be expected to yield the best MMM profile.

Despite of this conjecture, merely KP and TP model microfields have been considered in the present work for a weighty practical reason: $\gamma(t|E)$ is not known for the true microfield, and its calculation is certainly a task of its own. Thus, it seems to be advisable to investigate a problem more simple than Stark broadening first to test whether an adapted choice of the renewal process indeed improves the MMM.

Acknowledgement

I want to thank my wife, Helga Seidel, for drawing the figures.

[1] J. Holtsmark, Ann. Physik **58**, 577 (1919).
[2] H. R. Griem, Spectral Line Broadening by Plasmas, Academic Press, New York 1974.
[3] D. E. Kelleher and W. L. Wiese, Phys. Rev. Lett. **31**, 1431 (1973).
[4] W. L. Wiese, D. E. Kelleher, and V. Helbig, Phys. Rev. A **11**, 1854 (1975).
[5] H. Ehrich and D. E. Kelleher, Phys. Rev. A **17**, 1686 (1978).
[6] H. Ehrich and D. E. Kelleher, Phys. Rev. A **21**, 319 (1980).
[7] J. L. Chotin, J. L. Lemaire, J. P. Marque, and F. Rostas, J. Phys. B **11**, 371 (1978).
[8] H. Ehrich, Z. Naturforsch. **34a**, 188 (1979).
[9] C. Fleurier, G. Coulaud, P. Ranson, and J. Chapelle, Phys. Rev. A **21**, 851 (1980).
[10] K. Grützmacher and B. Wende, Phys. Rev. A **16**, 243 (1977).
[11] C. R. Vidal, J. Cooper, and E. W. Smith, Astrophys. J. Suppl. **25**, 37 (1973).
[12] K. Grützmacher and B. Wende, Phys. Rev. A **18**, 2140 (1978).
[13] R. Stamm and D. Voslamber, J. Quant. Spectrosc. Radiat. Transfer **22**, 599 (1979).
[14] J. Cooper, E. W. Smith, and C. R. Vidal, J. Phys. B **7**, L 101 (1974).
[15] D. Voslamber, Phys. Lett. **61A**, 27 (1977).
[16] A. V. Demura, V. S. Lisitza, and G. V. Sholin, Sov. Phys. JETP **46**, 209 (1977).
[17] J. Seidel, Z. Naturforsch. **32a**, 1207 (1977).
[18] H. R. Griem, Phys. Rev. A **17**, 214 (1978).
[19] R. W. Lee, J. Phys. B **11**, L 167 (1978).
[20] R. W. Lee, J. Phys. B **12**, 1145 (1979).
[21] R. L. Greene, Phys. Rev. A **19**, 2002 (1979).
[22] H. R. Griem, Phys. Rev. A **20**, 606 (1979).
[23] A. Brissaud and U. Frisch, J. Quant. Spectrosc. Radiat. Transfer **11**, 1767 (1971).
[24] A. Brissaud and U. Frisch, J. Math. Phys. **15**, 524 (1974).
[25] A. Brissaud, C. Goldbach, J. Léorat, A. Mazure, and G. Nollez, J. Phys. B **9**, 1147 (1976).
[26] A. Mazure and G. Nollez, Z. Naturforsch. **33a**, 1575 (1978).
[27] J. Seidel, in: Invited Papers for the 4th Int. Conf. on Spectral Line Shapes (ed. by W. E. Baylis), Univ. of Windsor (Canada) 1979.
[28] J. Seidel, Z. Naturforsch. **32a**, 1195 (1977).
[29] J. Seidel, Thesis, Univ. Düsseldorf 1974.
[30] J. Seidel. Z. Naturforsch. **34a**, 1385 (1979).
[31] T. W. Hussey, J. W. Dufty, and C. F. Hooper, Phys. Rev. A **16**, 1248 (1977).
[32] A. Brissaud, C. Goldbach, J. Léorat, A. Mazure, and G. Nollez, J. Phys. B **9**, 1129 (1976).
[33] H. A. Bethe and E. E. Salpeter, Quantum Mechanics of One- and Two-Electron Atoms, Springer-Verlag, Berlin 1957.
[34] M. Baranger and B. Mozer, Phys. Rev. **115**, 521 (1959)
[35] B. Mozer and M. Baranger, Phys. Rev. **118**, 626 (1960).
[36] C. F. Hooper, Phys. Rev. **149**, 77 (1966).
[37] C. F. Hooper, Phys. Rev. **165**, 215 (1968).
[38] H. Pfennig and E. Trefftz, Z. Naturforsch. **21a**, 697 (1966).